



## Coronal mass ejections and their heliospheric consequences

N. Gopalswamy\*

*NASA Goddard Space Flight Center, Greenbelt, Maryland 20771, USA*

**Abstract.** This paper is concerned with the properties of coronal mass ejections (CMEs) that affect the heliosphere. The special populations of CMEs that drive shocks, accelerate solar energetic particles, and produce geomagnetic storms are discussed in comparison with the general population (all CMEs of cycle 23). It is shown that the average CME speeds of the special populations are larger than that of the general population by a factor in the range 2–3. The angular width of these CMEs is also generally large because most of the CMEs were halos. The October – November 2003 period produced a large number of energetic CMEs, two of which were of historical proportions. These extreme events are discussed in order to understand what one might expect from the Sun as the largest event, given the maximum area and magnetic field strength of the source active regions.

*Keywords :* Sun: CMEs – solar-terrestrial relations – Sun: heliosphere

### 1. Introduction

Even though CMEs were discovered in the early 1970s, it took about two decades to realize that CMEs are responsible for most of the major disturbances in the heliosphere (see e.g., Gosling 1993). The severest of geomagnetic storms and the largest of solar energetic particle (SEP) events have been shown to be caused by energetic CMEs. SEPs are produced when the CMEs drive strong shocks (see e.g., Reames 1999), while intense geomagnetic storms are caused by the impact of the magnetized CME plasma on the magnetosphere (see e.g., Tsurutani et al. 1988). Early works that investigated the relation between CMEs and geomagnetic storms concentrated mainly on the interplanetary counterparts of CMEs (ICMEs) without paying much attention to the CMEs near the Sun. Studies that connected CMEs observed by coronagraphs

---

\*email: nat.gopalswamy@nasa.gov

to shocks and ICMEs observed in situ began in the 1980s; the CME - ICME connection is now well established (Burlaga et al. 1982; Sheeley et al. 1985; Lindsay et al., 1999; Gopalswamy et al. 2000). Only after the advent of the coronagraphs on board the Solar and Heliospheric Observatory (SOHO) mission (Domingo, Fleck & Poland 1995) the connection to CMEs near the Sun became evident, especially those affecting Earth's space environment. As of this writing, more than a million images of the corona have been obtained by SOHO's Large Angle and Spectrometric Coronagraph (LASCO, Brueckner et al., 1995) telescopes C2 and C3; these images largely form the basis for the current knowledge on CMEs and their heliospheric consequences. The Extreme-ultraviolet Imaging Telescope (EIT, Delaboudinière et al. 1995) on board SOHO became the workhorse in identifying the solar sources of CMEs. The Solar TERrestrial RELations Observatory (STEREO, Kaiser et al. 2008) has been providing information on the three-dimensional nature of CMEs since 2006. EIT was turned off recently after the launch of the Solar Dynamics Observatory (SDO, Schwer et al., 2002), which images the corona at several EUV wavelengths with higher cadence and better spatial resolution.

The purpose of this paper is to highlight some of the recent results concerning CMEs and their heliospheric impact primarily based on SOHO data. The paper is organized as follows: section 2 provides an update on the basic properties of CMEs. Section 3 highlights the shock-driving capability of CMEs. Section 4 focuses on the CME origin of SEP events. Section 5 describes the CME link to severe geomagnetic storms via the southward magnetic field component and the speed of CMEs. Section 6 describes the extreme events of the solar cycle 23. Concluding remarks are given in Section 7.

## 2. CME Properties

CMEs originate from closed field regions on the Sun such as active regions and filament regions, where free energy is stored and released due to some instability that is not fully understood (see e.g., Forbes 2000). CMEs appear as large-scale coherent structures in coronagraphic field of view and show clear outward motion from the Sun. The coherent structure is spatially inhomogeneous showing a number of substructures, with different densities, temperatures, and magnetic field strengths. For slow CMEs, one can often see a three-part structure consisting of a bright front followed by a dark void and a bright core (Hundhausen 1993). The dark void has been interpreted as a magnetic flux rope. The bright core is the eruptive prominence. Fast CMEs often show a diffuse structure surrounding the bright front, which is interpreted as the compressed shock sheath ahead of the CME (Gopalswamy 2009; Gopalswamy et al. 2009a; Ontiveros & Vourlidas 2009). The shock structure may be useful in measuring the heliospheric magnetic field (Gopalswamy & Yashiro 2011).

**Kinematics:** The speed, angular width, and apparent acceleration are the basic attributes of a CME. The measured sky-plane speed from the SOHO coronagraphs

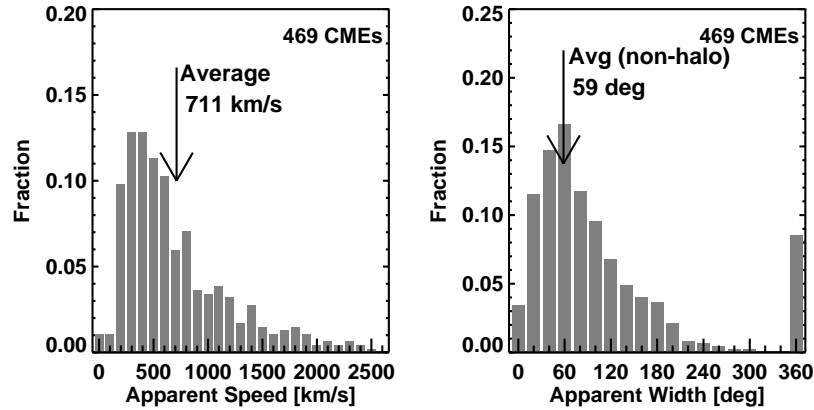


**Figure 1.** Speed and width distributions of LASCO CMEs associated with limb flares of X-ray importance  $\geq C3.0$ . The average width was computed using CMEs with width  $< 120^\circ$ .

(2.5 to 32 Rs field of view) ranges from less than 20 km/s to more than 3000 km/s. The angular width varies from a few degrees to more than  $120^\circ$ , with an average value of  $40^\circ$ . Fig. 1 shows the speed and width distributions of CMEs, which occurred close to the limb (within  $30^\circ$ ) and hence are subject to minimal projection effects. The limb events are chosen based on the association with soft X-ray flares of importance  $\geq C3$ . The limb CMEs are certainly faster (average speed  $\sim 700$  km/s) and wider (average non-halo width  $\sim 60^\circ$ ) compared to the general population (Gopalswamy 2010a). The set of limb CMEs used here has a slight bias towards energetic CMEs because of the soft X-ray flare level considered. The acceleration is speed dependent, generally in the range  $-50$  to  $50$  m s $^{-2}$ . Slow CMEs show acceleration and fast CMEs show deceleration within the coronagraphic field of view. For the limb CMEs, the average acceleration is  $\sim -3$  m s $^{-2}$ . It must be pointed out that the acceleration measured in the coronagraphic field of view ( $\geq 2.5$  Rs) is mainly due to the aerodynamic drag because the propelling force and gravity typically become insignificant by the time the CME reaches the outer corona. Initial acceleration seems to peak below this height (Wood et al. 1999; Gopalswamy & Thompson 2000; Zhang et al. 2001; Vrřnak 2001) with values two to three orders of magnitude higher than the deceleration due to drag (but of opposite sign).

**Mass and kinetic energy:** The CME mass ( $M$ ), estimated from LASCO data (see, e.g., Vourlidas et al. 2010) ranges from  $< 10^{12}$  g to  $> 10^{16}$  g with a median value of  $\sim 3.2 \times 10^{14}$  g. The estimated mass and speed can be used to get the CME kinetic energy, which ranges from  $< 10^{26}$  to  $> 10^{33}$  erg, with a median value of  $2.0 \times 10^{29}$  erg (Gopalswamy 2010a). For limb CMEs, the average mass and kinetic energy are  $1.3 \times 10^{15}$  g and  $1.6 \times 10^{29}$  erg, respectively. The higher values are consistent with pre-SOHO values (see e.g., Howard et al. 1985) obtained from less sensitive coronagraphs. The mass ( $M$  in g), width ( $W$  in degrees), and speed ( $V$  in km/s) of CMEs are

related (Gopalswamy et al. 2005c;2009b):

$$\log M = 12.6 + 1.3 \log W \quad (1)$$

and

$$V = 360 + 3.64W. \quad (2)$$

Thus, faster and wider CMEs have a higher kinetic energy.

**Occurrence rate and solar cycle variation:** Solar cycle 23 started around May 1996, while cycle 24 started around January 2009. Counting all the CMEs detected, we get ~14000 CMEs during cycle 23. This number is not exact because of data gaps, especially the long one in 1998 when SOHO was temporarily disabled. This gives an average rate of 1100 CMEs per year, but there is a solar-cycle variation of the occurrence rate, as can be seen in Fig. 2. The daily rate (averaged over Carrington rotation periods) varies by an order of magnitude between solar minimum and maximum. Also interesting is the variation of CME speed (again averaged over Carrington rotation periods) from ~200 km/s during solar minimum to ~600 km/s during the maximum. The spikes in the speed plot are due to some super active regions that produced large numbers of fast CMEs. It is clear that the Sun puts out more energetic CMEs during the solar maximum. During the cycle 23/24 minimum, the average CME speed reaches ~150 km/s, which is ~25% lower than that during the cycle 22/23 minimum. The solar wind is known to be slower during this period, but it is surprising that the CMEs are also of lower speed on the average. All CMEs have heliospheric consequences, but the ones causing noticeable changes are very energetic. One of the indicators of such CMEs is that they remain visible to the outer edge of the coronagraphic field of view. In order to isolate such CMEs, we have shown the speed and width distributions of CMEs that reach at least 20 Rs in Fig. 3. During the interval 1996 to 2010 (inclusive), nearly 16,000 CMEs have been detected. Only 15% of the CMEs remain bright enough to be measured to at least 20 Rs. We call these “bright CMEs”. The average speed of this population is 661 km/s, which is ~47% higher than the 450 km/s for the general population. Similarly, the average width (63°) is 57% higher than the 40° for the general population. Faster and wider CMEs on the average have more energy and hence travel farther into the interplanetary medium and affect the heliosphere in a number of ways.

One of the interesting features in Fig. 3 is the last bin in the width distribution: ~11% of the bright CMEs had a width of 360°. Such CMEs are known as ‘halo CMEs’ because they appear to surround the Sun in the sky plane (Howard et al. 1982). In reality, the halo CMEs are like other CMEs, except that they travel roughly along the Sun-Earth line and are generally more energetic. One has to use coronal images in X-ray, EUV, microwave, or chromospheric images in H-alpha to identify the source regions of CMEs. The fraction of halos in a CME population serves as a measure of the average energy of the population (Gopalswamy et al. 2010a). The true width of halo CMEs is unknown, but stereoscopic observations of the same CME from orthogonal views indicate that the width is generally well above average (>60°). As we noted in

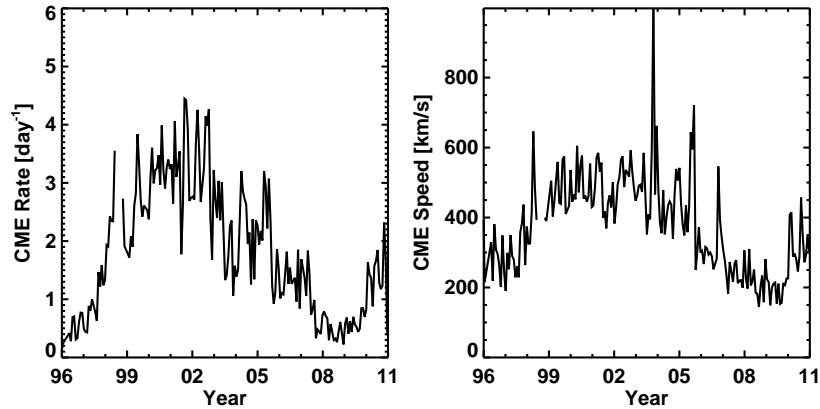


**Figure 2.** Variation of CME occurrence rate and speed (averaged over Carrington rotation periods) as a function of time. In the plot of CME rate versus year, only CMEs with width  $\geq 30^\circ$  are considered. Adapted from Gopalswamy et al., (2010c).

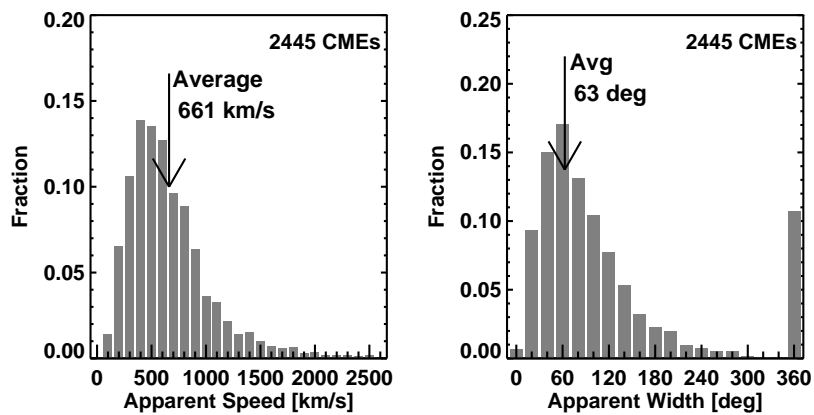


**Figure 3.** Speed and width distributions of CMEs for which height-time measurements can be made at least for 20 Rs (bright CMEs). The average width was computed counting only CMEs with width  $< 120^\circ$ . All measurements are with respect to the sky plane.

Eq. (2), wider CMEs are also faster and hence more energetic. The average speed of halo CMEs exceeds 1000 km/s, which is more than two times the average speed of the general population. In the following sections, we discuss special populations of CMEs that have significant heliospheric consequences and in each case, the halo CME fraction is much larger than that in the general population (3%).

**CMEs and Flares:** CME eruptions are almost always accompanied by a solar flare observed in X-rays (see e.g., Yashiro et al. 2008). However, not all flares are associated with CMEs: even some X-class flares have been found to lack CME asso-

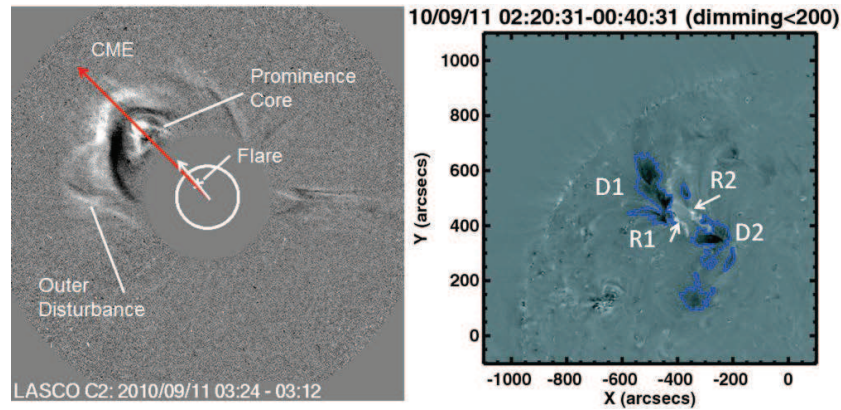


**Figure 4.** SOHO/LASCO CME on 2010 September 11 (left) associated with a filament eruption and a two-ribbon flare (right) observed by SDO/AIA at  $304 \text{ \AA}$ . The filament became the CME core. The flare (marked by asterisk) and the CME central position angle almost coincide in sky-plane projection. The outer disturbance can be seen on the north and south of the main body of the CME (flux rope). The outermost disturbance corresponds to EUV waves in the inner corona or a shock if the CME is very fast. Flare ribbons R1 and R2 and the dimming regions D1 and D2 in the eruption region are marked. The legs of the CME flux rope are thought to be rooted in D1 and D2.

ciation (Gopalswamy et al. 2009c). There is also a weak relationship between CME kinetic energy and peak X-ray flux (Hundhausen 1997). However, there is a large scatter, suggesting that there is an event-to-event variation in the fraction of free energy that goes into flare heating and mass motion. The physical connection between flares and CMEs is that the formation of the CME flux rope and the flare arcade (loops connecting the flare ribbons) are due to the same physical process, viz., flare reconnection (see e.g., Qiu et al. 2007). This has also been the central idea of the CSHKP standard solar flare model (Hanaoka et al. 1994). The CME speed evolution has been found to be similar to the associated soft X-ray profile, suggesting that the CME acceleration occurs largely during the rise phase of the flare (Wood et al., 1999; Zhang et al. 2001; Zhang & Dere 2006) analogous to the Neupert effect (the hard X-ray time profile is similar to the derivative of the soft X-ray light curve). Despite the inconclusive pre-SOHO results regarding the CME-flare positional correspondence, SOHO observations have shown that the CME nose is generally located radially above the flare location (Yashiro et al. 2008). Fig. 4 shows an example with the CME overlying the eruption region observed by SDO. The exceptions are the CMEs during the solar minimum phase when the CME nose is systematically off-set with respect to the eruption site because of the CME deflection towards the equator due to the strong field in the polar coronal holes (Gopalswamy et al. 2003). Finally, Moore, Sterling & Suess (2007) have shown that the geometrical size of the CME is also related to the flare magnetic flux (flare area times the average photospheric magnetic field within the area).

### 3. Shock-driving CMEs

The ability of CMEs to drive fast mode MHD shocks (when the CME speed exceeds the Alfvén speed in the corona and IP medium) has important space weather consequences. Shocks accelerate SEPs near the Sun and in the IP medium; shocks also cause the energetic storm particle (ESP) events and sudden commencement (SC) of geomagnetic storms. In a statistical study involving HELIOS in situ data and Solwind coronagraphic data, Sheeley et al. (1985) showed that most of the interplanetary shocks can in fact be traced to white-light CMEs observed near the Sun. Type II radio bursts are excellent indicators of CME-driven shocks (Robinson et al. 1985; Cane, Sheeley & Howard 1987; Gopalswamy et al. 2001). Type II bursts are produced by non-thermal electrons accelerated at the shock front via the plasma emission mechanism involving the generation of high-frequency plasma waves and their conversion to electromagnetic radiation at the fundamental and harmonic of the plasma frequency. As the shock moves away from the Sun, the plasma emission occurs at progressively lower frequencies causing the slow drift in the frequency - time plane (the so-called dynamic spectrum). Energetic CMEs obviously can drive shocks far into the IP medium, so the frequency range over which type II bursts occur depends on the CME kinetic energy, represented by the CME speed and the fraction of halos. CMEs with type II bursts extending to the lowest frequencies (tens of kHz, corresponding to the plasma frequency in the vicinity of the observing spacecraft) are the most energetic ones. The starting frequency of type II bursts is typically 150 MHz, although higher starting frequencies are occasionally observed (Vršnak et al. 1995). The starting frequency is determined by the local Alfvén speed and the CME speed. Fig. 5 shows the speed and width distributions of CMEs associated with type II bursts occurring only at metric (m) wavelengths (left panels) and in decameter-hectometric (DH) wavelengths (right panels). The m-type II bursts imply a shock very close to the Sun (within a solar radius above the surface); the shock might become radio quiet (no type II emission) or decay at larger distances. In the case of DH type II bursts, the shock continues into the IP medium. Clearly CMEs producing type II bursts in the interplanetary medium have greater speeds and larger fraction of wide CMEs, confirming that these CMEs are very energetic. In fact, CMEs producing type II bursts in all wavelength domains (from metric to DH to kilometric) are the most energetic with an average speed of  $\sim 1500$  km/s (Gopalswamy 2006). Sometimes type II bursts are observed only in the km domain. These CMEs remain too slow near the Sun but continue to accelerate and attain super-Alfvénic speeds at large distances from the Sun, where they drive shocks and produce type II bursts (Gopalswamy et al. 2010b). Such CMEs have an average speed similar to that of CMEs producing metric type II bursts, but with a different kinematics: the CMEs have positive acceleration within the coronagraphic field of view, compared to deceleration for the ones producing metric type II bursts. The low-speed CMEs in Fig. 5 associated with type II bursts indicate that occasionally the coronal Alfvén speed is very low enabling CMEs with speeds in the range 300-400 km/s to drive shocks and produce type II bursts. On the other hand some CMEs as fast as 1600 km/s are not associated with type II bursts, which

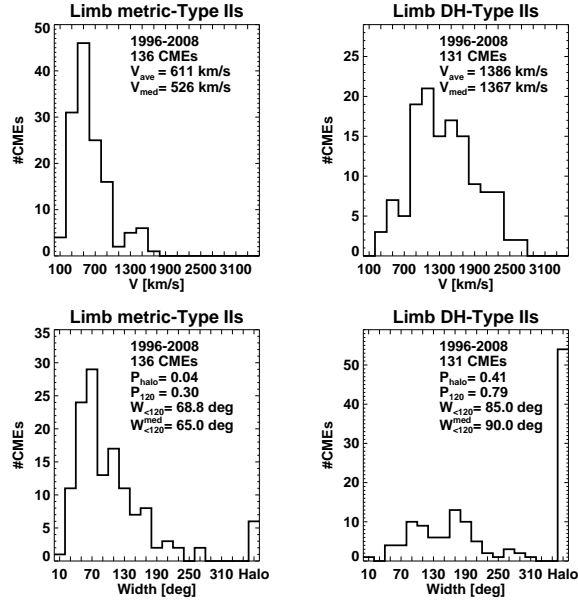


**Figure 5.** Speed and width distributions of limb CMEs associated with purely metric type II bursts (left) and DH type II bursts (right). The average and median speeds and the fraction of halos are noted.

can be explained by a tenuous corona with high Alfvén speeds so the CMEs remain sub-Alfvénic (Gopalswamy et al. 2008a). Thus, a CME originating from close to the disk center is highly likely to result in a shock arriving at Earth. It has been shown that about two thirds of IP shocks are radio loud (they produce type II bursts near the Sun or in the IP medium – see Gopalswamy et al. 2010b). However, about a third of shocks detected at 1 AU are associated with radio-quiet CMEs. These CMEs behave similar to the CMEs producing purely km type II bursts in that they continue to accelerate in the IP medium and drive shocks (Gopalswamy et al. 2005c), but the shocks are not strong enough to produce type II bursts. The CME kinematics and the ambient medium properties cause the observed variability in the IP shocks.

#### 4. CMEs and SEPs

Kahler, Hildner & Van Hollebeke (1978) found a close association between prompt SEP events and CMEs observed over a nine month period by Skylab, from which they concluded that the protons must be accelerated at the front of the CME-driven shocks. This was a crucial step in recognizing the important role played by CMEs in accelerating SEPs (see e.g., Gosling 1993; Reames 1999). The shock acceleration near the Sun is also consistent with the earlier suggestion that energetic particle flux increase around the time of geomagnetic storms is due to particles accelerated at the

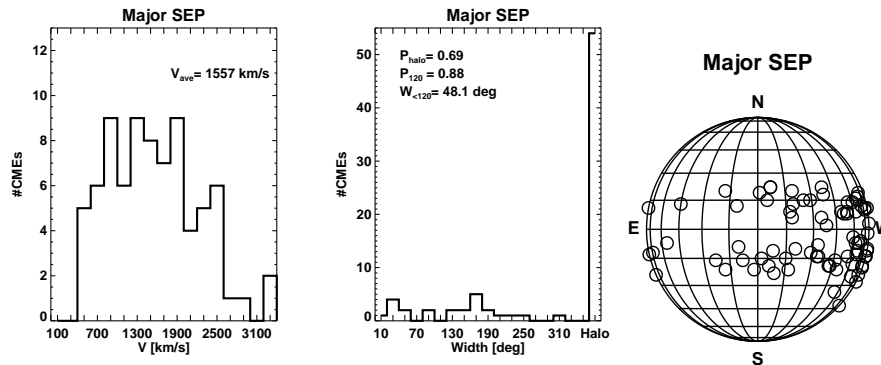


**Figure 6.** Speed, width, and source locations of LASCO CMEs associated with large (proton intensity  $\geq 10$  pfu in the  $> 10$  MeV channel) SEP events of solar cycle 23. Adapted from Gopalswamy et al., (2010c).

shock front passing the observing spacecraft near Earth (the so-called ESP events, see Rao, McCracken & Bukata 1968). The probability of association between type II radio bursts and SEP events increases when the radio bursts occur at longer wavelengths, implying shocks propagating into the IP medium (Cliver, Kahler & Reames 2004). The excellent set of simultaneous CME and SEP observations during cycle 23 showed that every large SEP event is associated with a fast and wide CME (Gopalswamy et al. 2002; Gopalswamy 2003), confirming the original suggestion by Kahler et al. (1978). Among various CME populations, the ones associated with SEPs seem to be the most energetic: the average speed of the SEP-producing CMEs exceeds 1500 km/s, compared to just 475 km/s for the general population of CMEs (Gopalswamy et al. 2009d). Fig. 6 shows that the CMEs are quite wide with 69% of them full halos and 88% partial or full halos. The solar sources are mostly located in the western hemisphere and originate from the active region belt, because only CMEs from active regions have very high energy. The occasional particle events from the eastern hemisphere are of low intensity but the associated CMEs are very energetic. The western bias of large SEP events is due to the well-known requirement for magnetic connectivity between the observer and the SEP source region (see e.g., Obayashi 1962). The source locations of type II bursts with emission components at all wavelengths are uniformly distributed in the disk (no western bias) because magnetic connectivity is not required (Gopalswamy et al. 2008b). The speed and width of the CMEs associated with such type II bursts are similar to the SEP-associated CMEs because the same shock accelerates electrons and ions.

The speed histogram in Fig. 6 shows that some slow CMEs (400 km/s) are associated with SEPs. On the other hand, some fast CMEs with speeds as high as 1600 km/s do not produce SEP events. These extremes point to the variability in the Alfvén speed in the corona (by a factor 4 from event to event). Thus a 500 km/s CME can be super-Alfvénic, while a 1600 km/s CME can be sub-Alfvénic depending on the ambient Alfvén speed. A combination of shock and ambient medium parameters needs

to be conducive for SEP production. Under favorable circumstances,  $\sim 10\%$  of CME kinetic energy may go into SEPs (Mewaldt 2006), suggesting that CME-driven shocks are very efficient particle accelerators. Despite this close connection, the correlation between SEP intensity and CME speed is less than perfect (Kahler & Hudson 2001). We have already noted that the Alfvén speed variability is one of the factors affecting the shock strength and hence the SEP intensity. Other factors include the presence of seed particles and enhanced turbulence and shock strengthening due to preceding CMEs (Kahler 2001; Gopalswamy et al. 2004). The presence of coronal holes near the eruption region may affect the CME trajectory (Gopalswamy et al. 2009e) and hence the magnetic connectivity leading to SEP intensity variation.

## 5. CMEs and geomagnetic storms

A geomagnetic storm occurs when the interplanetary magnetic field originating from the Sun interacts with the Earth's field in the magnetopause. The interaction happens via magnetic reconnection, which requires the interplanetary magnetic field with a southward component ( $B_s$ ) to merge with the northward field in the magnetopause. The net result is the flow of solar wind energy into the magnetosphere and the enhancement of the ring current leading to the temporary reduction of the horizontal component of Earth's magnetic field, readily detected by ground based magnetometers as geomagnetic storms. The storm mechanism was first elucidated by Dungey (1961). It is customary to measure the strength of a geomagnetic storm using one of the geomagnetic indices such as the Dst index (hourly average of the terrestrial low-latitude horizontal magnetic field in nT). When there is no CME, the interplanetary field is generally in the ecliptic plane at Earth except for the fluctuating component due to Alfvénic fluctuations in the solar wind. CMEs naturally contain  $B_s$  because of their flux rope structure. If the CME drives a shock, then the sheath region between the flux rope and the shock may also contain  $B_s$ , leading to some structure in the Dst time profile. Large-scale interplanetary structures known as corotating interaction regions (CIRs) may also contain  $B_s$  and hence cause intense geomagnetic storms. CIRs form when the fast solar wind from coronal holes overtakes the slow solar wind ahead, resulting in the interface containing higher density, temperature, and magnetic field. The  $B_s$  in CIRs essentially arises from the enhancement of  $B_s$  in the Alfvénic fluctuations in the stream interface reaching values similar to those in CMEs (Gopalswamy 2008). Statistical studies have shown that the severest of geomagnetic storms (Dst < -150 nT) are always caused by CMEs, while weaker storms can be caused by both CMEs and CIRs (Richardson et al. 2006; Zhang et al. 2007). The CME link to the geomagnetic storms is evident from the empirical relationship between Dst and the product of  $B_s$  (nT) and the speed  $V$  (km/s) of the ICME structure (Gopalswamy et al. 2008c):

$$Dst = -0.01VB_s - 32. \quad (3)$$

Equation (3) represents the regression line obtained from a scatter plot between the maximum values of  $B_s$  within the magnetic cloud (MC) and the Dst index. The correlation coefficient was found to be 0.90 for MCs and 0.86 for sheaths (Gopalswamy

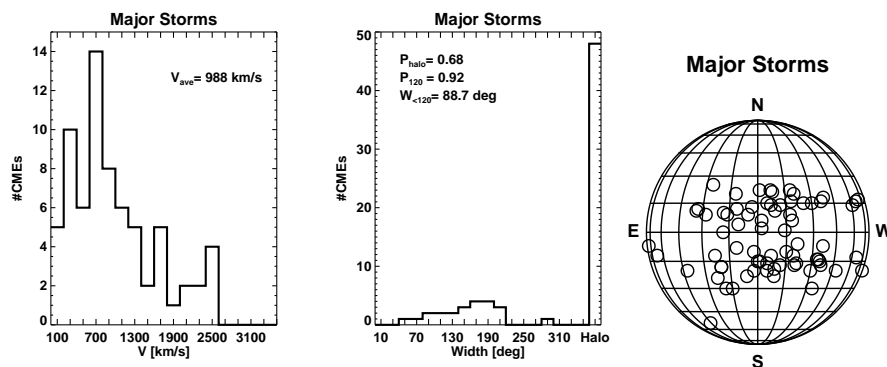


**Figure 7.** Speed (left), width (middle), and solar source location (right) of LASCO CMEs that cause major ( $Dst \leq 100 \text{ nT}$ ) geomagnetic storms during 1996 – 2006 (inclusive). The average CME speed ( $V_{ave}$ ) is 988 km/s. The fraction of full halos,  $P_{halo} = 68\%$ . Almost all (92%) CMEs have width  $\geq 120^\circ$ . Adapted from Gopalswamy (2010b).

2008). For storms produced by sheaths, the constant term in equation (1) is 14. Without Bs, even very fast CMEs cannot produce a geomagnetic storm because the CME field does not couple to the Earth's magnetic field. One of the famous examples is the 2003 October 30 super storm (Gopalswamy 2009) produced by the sheath, while the magnetic field in the cloud portion was pointing north throughout the cloud. Once the CME has Bs, faster CMEs produce more intense storms. Both the enhanced magnetic field and the kinetic energy of CMEs are ultimately related to the free energy in the solar source regions from which the CMEs originate (Gopalswamy 2010b; Gopalswamy et al. 2010c). Fig. 7 illustrates the importance of speed and width of CMEs that cause major geomagnetic storms. The average CME speed is  $\sim 1000 \text{ km/s}$  and most of the CMEs are halos or partial halos (92%). The average width of the remaining 8% of the CMEs is also large ( $\sim 89^\circ$ ). One of the basic requirements for CMEs to produce a geomagnetic storm is that they should hit Earth's magnetosphere. Statistical studies have shown that CMEs generally propagate radially above the source region (Yashiro et al. 2008), so CMEs need to originate close to the disk center of the Sun in order to arrive at Earth (Srivastava & Venkatakrishnan 2004). The width of CMEs causing geomagnetic storms typically exceed  $60^\circ$  (see Fig. 7) so the solar sources need to be located within a central meridian distance (CMD) of  $\sim 30^\circ$ . When the CME originates beyond  $30^\circ$ , only a small section of the CME might arrive at Earth or none at all, depending on the angular extent of the CMEs. Fig. 7 shows that most of the sources of CMEs causing intense storms are located within CMD  $\sim 30^\circ$ . The difference in the halo fractions and speeds between SEP and storm-producing CMEs may be partly due to the different source location distributions and hence different projection effects.

A statistical study of  $\sim 400$  halo CMEs found that the vast majority (71%) of the front-side halos were geoeffective (Gopalswamy et al. 2007); nearly half of the disk halos ( $CMD \leq 45^\circ$ ) resulted in intense storms ( $Dst \leq -100 \text{ nT}$ ), while another 26% were moderately geoeffective ( $-50 \leq Dst < -100 \text{ nT}$ ). About 25% of the disk halos

were not geoeffective ( $Dst > -50$  nT). High-inclination flux ropes with northward axial field, CME interaction and merging, and unusual deflection of CMEs away from the Sun-Earth line are likely reasons why these halos may not be geoeffective. Only 27% of the limb halos ( $CMD > 45^\circ$ ) were strongly geoeffective and 32% were moderately geoeffective. The backside halos were not geoeffective at all, as expected. About 40% of limb halos were non-geoeffective mainly because the associated flux ropes may not arrive at Earth. If the limb halos are geoeffective the cause is the sheath ahead of the CMEs. Gopalswamy et al. (2010d) examined the solar wind signatures of 17 limb halos associated with intense geomagnetic storms and found that five halos occurred around the time of other disk halos that caused the storms. In three cases, the halos produced perturbations in the recovery phases of other storms. Thus only 9 limb halos resulted in 7 intense geomagnetic storms (in three cases CME interaction was involved). It was confirmed that the geomagnetic storms following limb halos are indeed due to sheaths. Since the sheath is the first feature encountered by Earth's magnetosphere, the delay time between the onset of halo CMEs and the peak of ensuing geomagnetic storms is  $\sim 20\%$  smaller for limb halos. This study also revealed that two limb halos originating very close to the east limb (S07E80 on 2003 June 15 and S12E67 on 2005 September 9) resulted in large geomagnetic storms ( $-141$  and  $-147$  nT, respectively), but the CMEs were superfast (2053 km/s and 2257 km/s, respectively). Interestingly, the seven storms caused by limb halos are included in the 75 intense storms of solar cycle 23 (see Zhang et al. 2007) indicating that  $\sim 9\%$  of the intense storms are due to limb halos. Since  $B_s$  and  $V$  are the most important parameters that determine the strength of the geomagnetic storms, it is highly beneficial to estimate these quantities near the Sun. Currently one can easily estimate the speed of the CMEs near the Sun and the solar source location. For example, one can obtain the earthward speed of CMEs from the sky-plane measurements using (i) a cone model (Xie et al. 2006), (ii) flux-rope fitting (Thernisien et al. 2009), or (iii) the relation between radial and expansion speeds (Dal Lago et al. 2003; Gopalswamy et al. 2009c). However, determining  $B_s$  from solar observations is far from reality. By examining the neutral line in the source active region at the Sun, one may be able to qualitatively infer the internal structure of ICMEs, such as the inclination of the flux rope, expected direction of rotation, and the portion of the flux rope where  $B_s$  might occur (see e.g., Yurchyshyn, Hu & Abramenko 2005). In addition to deriving kinematics of CMEs from flux rope fitting, it may be possible to obtain the magnetic structure using a semi-analytic erupting flux-rope model (Kunkel & Chen 2010). The close connection between flare structure and flux rope structure in CMEs needs to be exploited (Qiu et al. 2007; Moore et al. 2007; Chen & Kunkel 2010) in arriving at a quantitative estimate of the magnetic content of CMEs before they arrive at Earth.

## 6. Extreme events

The four largest spikes in the CME speed in Fig. 2 correspond to CMEs from some super active regions on the Sun. Many of these CMEs may be regarded as extreme events. An extreme event can be defined as an occurrence, which is singularly unique

either in the occurrence itself or in terms of its consequences. The largest spike in Fig. 2 corresponds to the October - November 2003 period studied extensively (see Gopalswamy et al. 2005a for a list of 70 papers published on these events). The violent solar eruptions can be regarded as extreme events in terms of their origin as well as their heliospheric consequences. These eruptions involved the largest active region area of the solar cycle, the largest X-ray flare, the highest concentration of ultrafast ( $\geq 2000$  km/s) CMEs, the largest SEP event, the fastest IP shock, the highest concentration of IP radio bursts, and the highest solar wind speed. Two halo CMEs resulted in shocks that arrived at Earth in  $< 24$  hours. Historically, there were only 15 such fast-transit events, including the Carrington event of 1859 September 1. The two halos also resulted in super-intense geomagnetic storms (peak Dst index at - 363 and - 401 nT). This period also had the distinction of producing three ground level enhancement (GLE) events from a single active region (AR 10486). The four speed spikes in Fig. 2 in fact account for 8 of the 16 GLE events in cycle 23. The first three spikes accounted for at least two GLEs each and the smallest spike in 2006 accounted for just one GLE. Details on the super active regions of cycle 23 can be found in Gopalswamy et al. (2006).

The severe heliospheric impact of CMEs was best demonstrated by a series of eruptions from three active regions during October - November 2003, known as the Halloween 2003 events (Gopalswamy et al. 2005a,b). CMEs from this period were observed to arrive at Earth and progressively at Mars, Jupiter, Saturn, and all the way to the edge of the solar system. (Lario et al. 2005; McKibben et al. 2005; Crider et al. 2005; Intriligator et al. 2005). Some level of adverse effects was felt by 59% of reporting spacecraft and 18% of their instrument groups (Barbieri & Mahmot 2004). Ironically, the Martian Radiation Experiment (MARIE) experiment on board the Mars Odyssey, which was supposed to measure the radiation environment of Mars, succumbed to the onslaught of radiation from these CMEs. The 2003 October 28 SEP event resulted in significant ozone depletion (50-70%) between 50 and 80 km above the ground (Jackman et al. 2005). The October 29 SEP event was observed on board a commercial airplane from Los Angeles to New York. The observation demonstrated that the crew and passengers on the plane were subject to an equivalent dosage that was higher by  $\sim 37\%$  (Getley 2004). A ten-fold enhancement in the ionospheric total electron content over the US mainland occurred during 2003 October 30-31. Extraordinary density enhancements in both the magnetosphere and ionosphere coinciding with intervals of southward interplanetary magnetic field and high-speed solar wind were observed. A single merged interaction region formed out of the October/November 2003 CMEs that reached Voyager 2 after  $\sim 180$  days and produced a large depression in cosmic ray intensity, lasting more than 70 days. Fortunately, the large array of space and ground based instruments helped us not to be taken by surprise by these events, but to benchmark the extreme space weather events.

The cumulative distribution in Fig. 8 shows that the number of CMEs with speeds  $> 3000$  km/s is exceedingly small, probably due to the maximum amount of free energy available in source regions. Gopalswamy et al. (2010c) estimated an upper limit

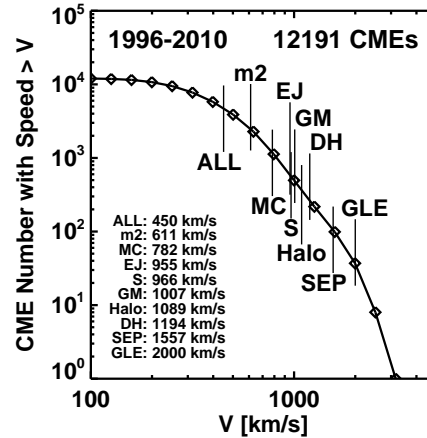


**Figure 8.** The cumulative distribution of CME speeds with the average speed of several CME populations marked: the general population(All), CMEs associated with metric (m2) and DH type II bursts, magnetic clouds (MC), ejecta (EJ), interplanetary shocks (S), geomagnetic storms (GM), SEPs and GLEs. The average speed of halo CMEs is also shown. All the special populations are of above average speed. The GLEs are a subset of SEP events with particles attaining  $\sim$  GeV energies and are associated CMEs of the highest speed. Adapted from Gopalswamy et al., (2010c).

of  $10^{36}$  erg for the potential energy in a hypothetical active region with the largest reported active region area (5000 millionths of a solar hemisphere, msh) and the maximum measured sunspot magnetic field (6100 G). The maximum free energy that can be stored in the active region is likely to be of the same order. If all the energy goes into a single CME, say of mass  $10^{18}$  g, the CME speed can exceed 14000 km/s. A single CME may not exhaust all the free energy (the CME recurrence time in large active regions is much smaller than the time taken to build up the free energy). For the 2003 October 28 extreme events, Gopalswamy et al. (2005b) estimated that the CME kinetic energy represented 5 to 26% of the potential energy. Taking the maximum value, one can estimate a maximum CME speed of  $\sim$ 7200 km/s, which is about two times the maximum observed speed. Such a CME would travel to Earth in  $\sim$ 11.6 hours according to the empirical shock arrival model (Gopalswamy et al., 2005b).

## 7. Concluding remarks

Coronal mass ejections are a relatively new phenomenon compared to the solar activity known for centuries. The preeminent role of CMEs in the solar terrestrial relationship became clear only in the 1990s. Rapid progress in CME research became possible only after the SOHO mission was launched in December 1995. We have nearly continuous data on CMEs for the whole of solar cycle 23 and part of cycle 24.

The importance of CMEs in longer time-scale phenomena such as the modulation of galactic cosmic rays can be understood only after a magnetic cycle. Along with the observations, significant effort has also gone into MHD modeling of the CMEs from their initiation to interplanetary propagation. Despite the enormous progress, we do not fully understand the CME initiation. We are still not able to tell with confidence when and where a CME will take place in an active region or a filament region. We have just begun to understand how the flux rope structure in a CME comes about, but still there is debate as to whether they form during the eruption or exist before the eruption. Finally, we must point out that the statistical results on CMEs presented in this paper do not account for the fact that the leading edge of fast CMEs may be a shock, rather than the frontal structure. This is a recent revelation, so the statistical results may have to be revised by separating shock-driving CMEs and non-shock CMEs.

### Acknowledgements

The author thanks S. Yashiro and P. Mäkelä for help with the figures. Work supported by NASA LWS/TR&T program.

### References

- Barbieri L. P., Mahmot R. E., 2004, *SpWea*, 2, S09002  
Brueckner G.E. et al. 1995, *Solar Phys.*, 162, 357  
Burlaga L. F., Klein L., Sheeley N. R., Jr., Michels D. J., Howard R. A., Koomen M. J., Schwenn R., Rosenbauer H., 1982, *GeoRL*, 9,1317  
Cane H. V., Sheeley N. R., Jr., Howard R. A., 1987, *JGR*, 92, 9869  
Chen J., Kunkel V., 2010, *ApJ*, 717, 1105  
Cliver E. W., Kahler S. W., Reames D. V., 2004, *ApJ*, 605, 902  
Crider D. H., Espley J., Brain D. A., Mitchell D. L., Connerney J. E. P., Acuña M. H., 2005, *JGRA*, 110, A09S21  
Dal Lago A., Schwenn R., Gonzalez W. D., 2003, *AdSpR*, 32, 2637  
Delaboudinière J.-P., et al., 1995, *Solar Phys.*, 162, 291  
Domingo V., Fleck B., Poland A., 1995, *Solar Phys.*, 162,1  
Dungey J. W., 1961, *PhRvL*, 6, 47  
Forbes T. G., 2000, *JGR*, 105, 23153  
Getley I. L., 2004, *SpWea*, 2, S05002  
Gopalswamy N., 2003, *GeoRL*, 30, 8013  
Gopalswamy N., 2004, in *The Sun and the Heliosphere as an Integrated System*, Eds G. Poletto and S. T. Suess, Vol. 317, Kluwer Academic Publishers, Dordrecht, The Netherlands, 2004, p.201  
Gopalswamy N., 2006, *Geophysical Monograph Series*, Vol. 165, Eds N. Gopalswamy, R. Mewaldt, and J. Torsti, AGU, 2006, p.207  
Gopalswamy N., 2008, *JASTP*, 70, 2078

- Gopalswamy, N., in *Climate and Weather of the Sun-Earth System (CAWSES)*, Eds T. Tsuda, R. Fujii, K. Shibata, and M. A. Geller, Terrapub, Tokyo, 2009, p. 77
- Gopalswamy N., 2010a, *Proc. National Solar Physics Meeting*, Slovakia, Papradno, p. 108
- Gopalswamy N., 2010b, *IAUS*, 264, 326
- Gopalswamy N., et al., 2009a, *Solar Phys.*, 259, 227
- Gopalswamy N., Aguilar-Rodriguez E., Yashiro S., Nunes S., Kaiser M. L., Howard R. A., 2005c, *JGRA*, 110, A12S07
- Gopalswamy N., Akiyama S., Yashiro S., 2009c, *IAUS*, 257, 283
- Gopalswamy N., Akiyama S., Yashiro S., Michalek G., Lepping R. P., 2008c, *JASTP*, 70, 245
- Gopalswamy N., Akiyama S., Yashiro S., Mäkelä P., 2010c, in *Magnetic Coupling between the Interior and Atmosphere of the Sun*, eds. S. S. Hasan and R. J. Rutten, *Astrophysics and Space Science Proceedings*, p. 289
- Gopalswamy N., Barbieri L., Cliver E. W., Lu G., Plunkett S. P., Skoug R. M., 2005a, *JGRA*, 110, A09S00
- Gopalswamy N., Dal Lago A., Yashiro S., Akiyama S., 2009b, *CEAB*, 33, 115
- Gopalswamy N., Lara A., Lepping R. P., Kaiser M. L., Berdichevsky D., St. Cyr O. C., 2000, *GeoRL*, 27, 145
- Gopalswamy N., Xie H., Mäkelä P., Akiyama S., Yashiro S., Kaiser M. L., Howard R. A., Bougeret J.-L., 2010b, *ApJ*, 710, 1111
- Gopalswamy N., Mäkelä P., Xie H., Akiyama S., Yashiro S., 2009e, *JGRA*, 114, A00A02
- Gopalswamy N., Shimojo M., Lu W., Yashiro S., Shibasaki K., Howard R. A., 2003, *ApJ*, 586, 562
- Gopalswamy N., Thompson B. J., 2000, *JASTP*, 62, 1457
- Gopalswamy N., Yashiro S., 2011, *ApJ*, 736, L17
- Gopalswamy N., Yashiro S., Akiyama S., 2006, In *Proc. ILWS Workshop*, Goa, India, February 19-24, 2006, Eds N. Gopalswamy and A. Bhattacharyya, p.79
- Gopalswamy N., Yashiro S., Akiyama S., 2007, *JGRA*, 112, A06112
- Gopalswamy N., Yashiro S., Akiyama S., Mäkelä P., Xie H., Kaiser M. L., Howard R. A., Bougeret J. L., 2008b, *AnGeo*, 26,3033
- Gopalswamy N., Yashiro S., Kaiser M. L., Howard R. A., Bougeret J.-L., 2001, *JGR*, 106, 29219
- Gopalswamy N., Yashiro S., Krucker S., Stenborg G., Howard R. A., 2004, *JGRA*, 109, A12105
- Gopalswamy N., Yashiro S., Liu Y., Michalek G., Vourlidas A., Kaiser M. L., Howard R. A., 2005b, *JGRA*, 110, A09S15
- Gopalswamy N., Yashiro S., Michalek G., Kaiser M. L., Howard R. A., Reames D. V., Leske R., von Roseninge T., 2002, *ApJ*, 572, L103
- Gopalswamy N., Yashiro S., Michalek G., Xie H., Mäkelä P., Vourlidas A., Howard R. A., 2010a, *SunGe*, 5, 7
- Gopalswamy N., Yashiro S., Xie H., Akiyama S., Mäkelä P., 2010d, in *Advances in Geosciences*, Vol. 21: *Solar Terrestrial (ST)*, Ed M. Duldig, Singapore: World Scientific, 2010, p.71

- Gopalswamy N., Yashiro S., Michalek G., Stenborg G., Vourlidas A., Freeland S., Howard R., 2009d, *EM&P*, 104, 295
- Gopalswamy N., Yashiro S., Xie H., Akiyama S., Aguilar-Rodriguez E., Kaiser M. L., Howard R. A., Bougeret J.-L., 2008a, *ApJ*, 674, 560
- Gosling J. T., 1993, *JGR*, 98, 18937
- Hanaoka Y., et al., 1994, *PASJ*, 46, 205
- Howard R. A., Michels D. J., Sheeley N. R., Jr., Koomen M. J., 1982, *ApJ*, 263, L101
- Howard R. A., Sheeley N. R., Jr., Michels D. J., Koomen M. J., 1985, *JGR*, 90, 8173
- Hundhausen A. J., 1993, *JGR*, 98, 13177
- Hundhausen, A. J., 1997, in *Coronal Mass Ejections*, ed. N. Crooker, J. A. Joselyn, & J. Feynman, AGU Monograph 99, p. 1
- Intriligator D. S., Sun W., Dryer M., Fry C. D., Deehr C., Intriligator J., 2005, *JGRA*, 110, A09S10
- Jackman C. H., DeLand M. T., Labow G. J., Fleming E. L., Weisenstein D. K., Ko M. K. W., Sinnhuber M., Russell J. M., 2005, *JGRA*, 110, A09S27
- Kahler S. W., Hildner E., Van Hollebeke M. A. I., 1978, *Solar Phys.*, 57, 429
- Kahler S. W., Hudson H. S., 2001, *JGR*, 106, 29239
- Kaiser M. L., Kucera T. A., Davila J. M., St. Cyr O. C., Guhathakurta M., Christian E., 2008, *SSRv*, 136, 5
- Kunkel V., Chen J., 2010, *ApJ*, 715, L80
- Lario D., Decker R. B., Livi S., Krimigis S. M., Roelof E. C., Russell C. T., Fry C. D., 2005, *JGRA*, 110, A09S11
- Lindsay G. M., Luhmann J. G., Russell C. T., Gosling J. T., 1999, *JGR*, 104, 12515
- McKibben R. B., et al., 2005, *JGRA*, 110, A09S19
- Mewaldt R. A., 2006, *SSRv*, 124, 303
- Moore R. L., Sterling A. C., Suess S. T., 2007, *ApJ*, 668, 1221
- Obayashi T., 1962, *JPSJS*, 17, 572
- Ontiveros V., Vourlidas A., 2009, *ApJ*, 693, 267
- Qiu J., Hu Q., Howard T. A., Yurchyshyn V. B., 2007, *ApJ*, 659, 758
- Reames D. V., 1999, *SSRv*, 90, 413
- Rao U. R., McCracken K. G., Bukata R. P., 1968, *CaJPh*, 46, 844
- Richardson I. G., et al., 2006, *JGRA*, 111, A07S09
- Robinson R. D., 1985, *Solar Phys.*, 95, 343
- Schwer, K. Lilly, R. B., Thompson, B. J., Brewer, D. A., 2002, AGU Fall Meeting, abstract SH21C-01
- Sheeley N. R., Jr., Howard R. A., Michels D. J., Koomen M. J., Schwenn R., Muehlhaeuser K. H., Rosenbauer H., 1985, *JGR*, 90, 163
- Thernisien A., Vourlidas A., Howard R. A., 2009, *Solar Phys.*, 256, 111
- Tsurutani B. T., Smith E. J., Gonzalez W. D., Tang F., Akasofu S. I., 1988, *JGR*, 93, 8519
- Vourlidas A., Howard R. A., Esfandiari E., Patsourakos S., Yashiro S., Michalek G., 2010, *ApJ*, 722, 1522
- Vršnak B., 2001, *JGR*, 106, 25249
- Vršnak B., Ruzdjak V., Zlobec P., Aurass H., 1995, *Solar Phys.*, 158, 331
- Wood B. E., Karovska M., Chen J., Brueckner G. E., Cook J. W., Howard R. A., 1999,

- ApJ, 512, 484
- Xie H., Gopalswamy N., Ofman L., St. Cyr O. C., Michalek G., Lara A., Yashiro S., 2006, SpWea, 4, S10002
- Yashiro S., Michalek G., Akiyama S., Gopalswamy N., Howard R. A., 2008, ApJ, 673, 1174
- Yurchyshyn V., Hu Q., Abramenko V., 2005, SpWea, 30, S08C02
- Zhang J., Dere K. P., Howard R. A., Kundu M. R., White S. M., 2001, ApJ, 559, 452
- Zhang J., Dere K. P., 2006, ApJ, 649, 1100
- Zhang J., et al., 2007, JGRA, 112, A10102